sustainability

MDPI

Article

GIS-Based Frequency Ratio and Analytic Hierarchy Process for Forest Fire Susceptibility Mapping in the Western Region of Syria

Hazem Ghassan Abdo [1,2,3], Hussein Almohamad [4,*], Ahmed Abdullah Al Dughairi [4] and Motirh Al-Mutiry [5]

[1] Geography Department, Faculty of Arts and Humanities, University of Tartous, Tartous P.O. Box 2147, Syria; hazemabdo@tartous-univ.edu.sy
[2] Geography Department, Faculty of Arts and Humanities, University of Damascus, Damascus P.O. Box 30621, Syria
[3] Geography Department, Faculty of Arts and Humanities, University of Tishreen, Lattakia P.O. Box 2237, Syria
[4] Department of Geography, College of Arabic Language and Social Studies, Qassim University, Buraydah 51452, Saudi Arabia; adgierie@qu.edu.sa
[5] Department of Geography, College of Arts, Princess Nourah Bint Abdulrahman University, Riyadh 11671, Saudi Arabia; mkalmutairy@pnu.edu.sa
* Correspondence: h.almohamad@qu.edu.sa

Abstract: Forest fires are among the most major causes of global ecosystem degradation. The integration of spatial information from various sources using statistical analyses in the GIS environment is an original tool in managing the spread of forest fires, which is one of the most significant natural hazards in the western region of Syria. Moreover, the western region of Syria is characterized by a significant lack of data to assess forest fire susceptibility as one of the most significant consequences of the current war. This study aimed to conduct a performance comparison of frequency ratio (FR) and analytic hierarchy process (AHP) techniques in delineating the spatial distribution of forest fire susceptibility in the Al-Draikich region, located in the western region of Syria. An inventory map of historical forest fire events was produced by spatially digitizing 32 fire incidents during the summers of 2019, 2020, and 2021. The forest fire events were divided into a training dataset with 70% (22 events) and a test dataset with 30% (10 events). Subsequently, FR and AHP techniques were used to associate the training data set with the 13 driving factors: slope, aspect, curvature, elevation, Normalized Difference Vegetation Index (NDVI), Normalized Difference Moisture Index (NDMI), Topographic Wetness Index (TWI), rainfall, temperature, wind speed, TWI, and distance to settlements, rivers and roads. The accuracy of the maps resulting from the modeling process was checked using the validation dataset and receiver operating characteristics (ROC) curves with the area under the curve (AUC). The FR method with AUC = 0.864 achieved the highest value compared to the AHP method with AUC = 0.838. The outcomes of this assessment provide constructive spatial insights for adopting forest management strategies in the study area, especially in light of the consequences of the current war.

Keywords: forest fire susceptibility; frequency ratio; analytic hierarchy process; Syria

check for updates

Citation: Abdo, H.G.; Almohamad, H.; Al Dughairi, A.A.; Al-Mutiry, M. GIS-Based Frequency Ratio and Analytic Hierarchy Process for Forest Fire Susceptibility Mapping in the Western Region of Syria. *Sustainability* **2022**, *14*, 4668. https://doi.org/10.3390/su14084668

Academic Editors: Abolfazl Jaafari and Davood Mafi-Gholami

Received: 12 March 2022
Accepted: 12 April 2022
Published: 13 April 2022

Publisher's Note: MDPI stays neutral with regard to jurisdictional claims in published maps and institutional affiliations.

Copyright: © 2022 by the authors. Licensee MDPI, Basel, Switzerland. This article is an open access article distributed under the terms and conditions of the Creative Commons Attribution (CC BY) license (https://creativecommons.org/licenses/by/4.0/).

1. Introduction

Forests are one of the main natural resources that represent the safety valve of the global ecological balance and the sustainability of human civilization [1–4]. According to a report by the Food and Agriculture Organization (FAO), the global forest area constitutes 4.06 billion hectares (30.06%) of the Earth's surface area [5]. In addition to deforestation and forest degradation, forest fires are among the most critical threats to forest systems globally [6]. Forest fires are caused by natural causes such as lightning and volcanoes, or human causes, such as arson, accidents, the absence of relevant authorities, and military action [7,8]. However, the spatial response to fire incidents varies according to the different

topographic, climatic, biological, and human characteristics [9–11]. In this regard, forest fire events cause negative spatial impacts on biodiversity, ecological balance, wildlife, climate change, geophysical and geochemical processes, atmospheric and hydrological properties, soil, socio-economic and tourism productivity, and population well-being and health [12–14].

The Mediterranean region is characterized by a very diverse wild vegetation that preserves many endangered plant and animal species [15,16]. Moreover, forests represent one of the most important pillars of bio-economic life in the countries of the Mediterranean basin [17,18]. In the context of environmental change in the Mediterranean region, forest fires have recently been the biggest factor that has caused the degradation of large forest areas [19]. Spatial technologies such as geographic information systems (GIS) and remote sensing (RS) data, however, provide an advanced tool with reliable spatial outputs that effectively help in the management of fire risk, as indicated by several relevant studies [2,20]. Additionally, forest fire susceptibility maps produced by the integration of spatial techniques and statistical models represent one of the most common approaches to investigating the impact of physical and human geographical characteristics on forest fire propagation [1,21–23].

As a result of originality, diversity, high spatial density, socio-economic importance, and variation of natural geographical characteristics, forests are foremost among the environmental resources in the western region of Syria [24,25]. In this regard, more than 76% of the forest area in Syria is concentrated in its western region [24]. Forests in western Syria are acutely vulnerable to many manifestations of deterioration, especially high-frequency forest fire incidents. Plant structure, topographical and climatic characteristics, drought episodes, and lightning strikes, however, are among the most important physical factors driving the occurrence of forest fires in western Syria. Unsustainable tourism activity, coaling, wild cooking, and vandalism are among the most damaging human factors that contribute to the increase in the frequency of forest fire incidents [7].

Moreover, the western region of Syria experienced the most serious incidents of forest fires during the summers of 2019, 2020, and 2021 [26]. Those huge forest fires caused a massive loss of forest area, tragic destruction of many wild habitats, deaths, burning of homes, displacement of the population, and the total removal of many unique plant species, especially in the Al-Draikich area. Thus, the problem of forest fires represents a critical situation that requires a comprehensive spatial assessment of the susceptibility of forests to fire incidents in the study area.

Nowadays, mapping the spatial distribution of forest fire susceptibility is one of the most essential measures that render the management of this disaster at the national level. The integration of fieldwork, RS data, GIS techniques, and statistical methods can build reliable spatial prediction of the potential forest fire hazard area for different regions. Given the environmental threat posed by forest fires in the Al-Draikich area, the ultimate objective of this research is determined by the mapping of the spatial distribution of forest fire susceptibility in the study area by comparing the performance of the frequency ratio (FR) and analytic hierarchy process (AHP) techniques in producing the map of the current forest fire incident inventory with 13 forest fire-causing factors. In light of the paucity of national literature on in-depth studies of forest fires, the outputs of this study carry important values for local decision-makers to produce a set of spatial procedures and strategies that can contribute to managing this issue, especially in the post-war phase in Syria.

2. Material and Methods

2.1. Study Area

The Al-Draikich area is one of the six administrative regions in Tartous Governorate, western Syria, with an area of 186 km^2 representing 10% of the area of Tartous Governorate. The study area is geographically located between 34°58′ N to 35°10′ N latitude and 35°55′ E to 36°19′ E longitude (Figure 1). The Al-Draikich region is located in the east of the Tartus Governorate, where it is bordered by the Tartous city administrative region to the west, to

the north by the Sheikh Badr region, to the south by the Safita region, and to the east by the administrative borders with the Hama Governorate. Geomorphologically, the elevation in the Al-Draikich area ranges from 171 m to 1110 m. It can be divided into two terrain sectors [27]: The first sector is hilly, whose height ranges from 171 m to 400 m, and the second terrain sector includes the mountainous area, whose height ranges from 400 m to 1110 m. The study area is subject to the mountainous Mediterranean climate: the *Csa* and *Csb* patterns (Köppen climate classification), where the average annual temperature reaches 16.6 °C with a relative humidity of 67.4% and the annual rainfall rate reaches 1152 mm [24]. The wild plant system in the study area consists particularly of Oaks, Acacia, Terebinths, Carob, Brutia Pine, and Cypress [15,28]. The integration of physical and human geographical characteristics has made the study area highly vulnerable to forest fire incidents, especially in the dry season, which lasts for 6–7 months annually.

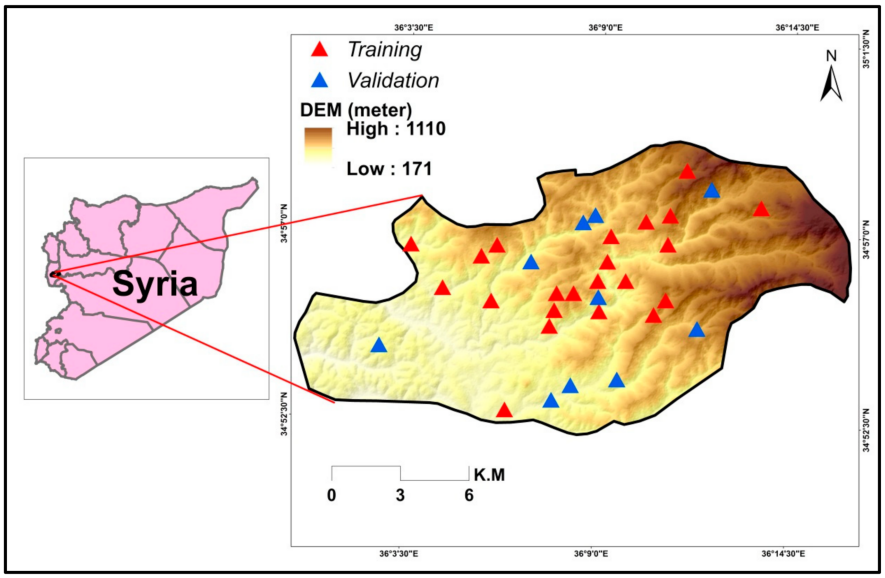

Figure 1. The location of the study area with training and validation sets of forest fires.

2.2. Data Used

The specific driving factors in this study imposed a multi-source data set, as shown in Table 1. A digital elevation model (DEM) obtained from the USGC earth explorer (https://earthexplorer.usgs.gov/) (accessed on 12 September 2021) was used to derive topographic and hydrologic data such as slope, elevation, curvature, aspects, drainages, and the Topographic Wetness Index (TWI). The spatial distribution of the Normalized Difference Vegetation Index (NDVI) and Normalized Difference Moisture Index (NDMI) values was mapped based on Landsat 8 (OLI-TIRS) data collected from the USGC EarthExplorer (https://earthexplorer.usgs.gov/) (accessed on 14 September 2021) [29–31]. Data obtained from the General Directorate of Meteorology in Damascus (GDM) provided the possibility of mapping the spatial distribution of the most influential climatic elements in stimulating forest fires, namely, rainfall, temperature, and wind speed.

The spatial distribution of climate-related factors was mapped using the interpolation techniques at a resolution of 30 m. Data of the Directorate of Transport in Tartous Governorate enabled the monitoring of the impact of the road network on stimulating the occurrence of forest fires. The distance to the road network was mapping with Euclidean distance tools at a resolution of 30 m. However, these data were entered and processed in the GIS environment (ArcMap 10.3) by using the spatial analysis tools in the software: resample, resize, Euclidean distance, interpolation, tabulation, conversion, raster calculator, and reclassification tools at a resolution of 30 m.

Table 1. Thematic layers of factors used and sources of data.

Factor	Data Source	Data Format	Resolution
Slope (deg.) Elevation (m) Curvature Aspect Drainages Topographic Wetness Index (TWI)	USGC EarthExplorer (https://earthexplorer.usgs.gov/) (accessed on 12 September 2021)	Spatial raster grid data	30 m
Settlements Normalized Difference Vegetation Index (NDVI) Normalized Difference Moisture Index (NDMI)	Landsat OLI-TIRS, August 2021 (USGS EarthExplorer) (accessed on 14 September 2021)	Spatial raster grid data	30 m
Rainfall (mm) Temperature (°C) Wind speed (m/s)	General Directorate of Meteorology—Damascus	Spatial vector data	-
Roads	Directorate of Transport and Public Roads—Tartous Governorate	Spatial vector data	-

Based on the fieldwork, the spatial specificity of the study area, the relevant previous literature, and the abundance of data, a number of driving factors were relied on upon modeling the forest fire sensitivity. These factors, however, have been reported in several relevant studies [6,9,21,32,33]. In a GIS environment, thematic layers representing the factors of forest fires were generated using data from various sources, especially remote sensing. The DEM with a resolution of 30 m used was projected to Universal Transverse Mercator (UTM) zone 37 with World Geodetic System 1984 (WGS 84). Using this projected DEM, maps of slope, elevation, curvature, aspects, and the drainage network were prepared. A spatial distribution of the Topographic Wetness Index (TWI) values was mapped using Equation (1).

$$\mathrm{TWI} = \ln\left(\frac{\mathrm{CA}}{\mathrm{Slope}}\right) \quad (1)$$

where CA determines the local upslope basin area and Slope outlines the steepest outward slope for each grid cell [34]. The Euclidean distance tool in the GIS software was used on the derivation maps of the distance to settlement, drainage, and road. NDVI and NDMI are among the most influential vital indicators of the presence and levels of moisture. Based on data obtained from the USGC EarthExplorer, NDVI and NDMI values were mapped using Equations (2) and (3).

$$\mathrm{NDVI} = \frac{\mathrm{NIR} - \mathrm{Red}}{\mathrm{NIR} + \mathrm{Red}} \quad (2)$$

$$\mathrm{NDVI} = \frac{\mathrm{SWIR} - \mathrm{NIR}}{\mathrm{SWIR} + \mathrm{NIR}} \quad (3)$$

where NIR represents the near-infrared band and SWIR represents the short-wave infrared band, as NDVI and NDMI are normalized indicators ranging between −1 and + 1 [35,36]. The inverse distance weighted (IDW) method was used in delineating the spatial distribution of rainfall, temperature, and wind speed values.

2.3. Forest Fire Inventory Map

Preparing a point inventory map of the spatial distribution of forest fire events is one of the critical initial procedures of spatial susceptibility mapping [1,2]. In the current study, the locations of forest fire ignition points during 2019, 2020, and 2021 were collected using extensive fieldwork and surveys of the Directorate of Agriculture in the Tartous Governorate (Figure 2). The observation period (the last three years), however, saw the most devastating fires in the study area [26]. These data were combined and digitized in

a GIS environment and a forest fire event inventory map was prepared. Figure 1 shows that 32 forest fire points had been spatially recorded across the study area. A total of 70% (22 points) of the total forest fire events were randomly assigned as training points that were calibrated with 13 forest fire-triggering factors using the FR and AHP methods. A total of 30% of the forest fire inventory events (10 points) were used to test the accuracy of the resulting maps [37].

Figure 2. Photographs showing forest fire events during the summers of 2019, 2020, and 2021.

2.4. Causative Factor Layers

Thirteen layers in the raster output representing the spatial factors stimulating forest fires in the study area were combined in the GIS environment using the FR and AHP methods. These cellular layers were classified using common spatial classification approaches, including *Natural Breaks*, *Equal interval-directional units*, and *Manual*.

2.4.1. Slope (S)

The slope is one of the most important factors, and has a positive impact on the increase of fire propagation [4,9]. Fire spread increases with a steep slope in high areas, in contrast to gentle slope forests that feature low susceptibility to fire [2]. In the current study, the slope degrees were categorized into six spatial classes (Figure 3a): <5°, 5–10°, 10–15°, 15–20°, 20–25°, and >25°.

2.4.2. Elevation (EI)

The elevation factor controls many topographic, climatic, and hydrologic parameters that affect the spread and intensity of forest fires, such as wind speed and direction, temperature, precipitation, humidity, and runoff [32,38]. Elevation also causes a critical spatial variation in the spread of forest fires at the level of patterns and types of vegetation cover and soil properties [10,39]. Thus, there is a direct relationship between an increase in forest fire events and an increase in elevation. The study-area elevation map was classified into five categories with an interval of 200 m (Figure 3b): <200, 200–400, 400–600, 600–800, and >800 m.

2.4.3. Curvature (CV)

The curvature is one of the topographic indicators that may control fire spread, depending on the change rate of the slope angle between negative slope (concave curvature) and positive (convex curvature) [32,40–42]. In the current assessment, curvature values were classified into three categories (Figure 3c): convex, flat, and concave.

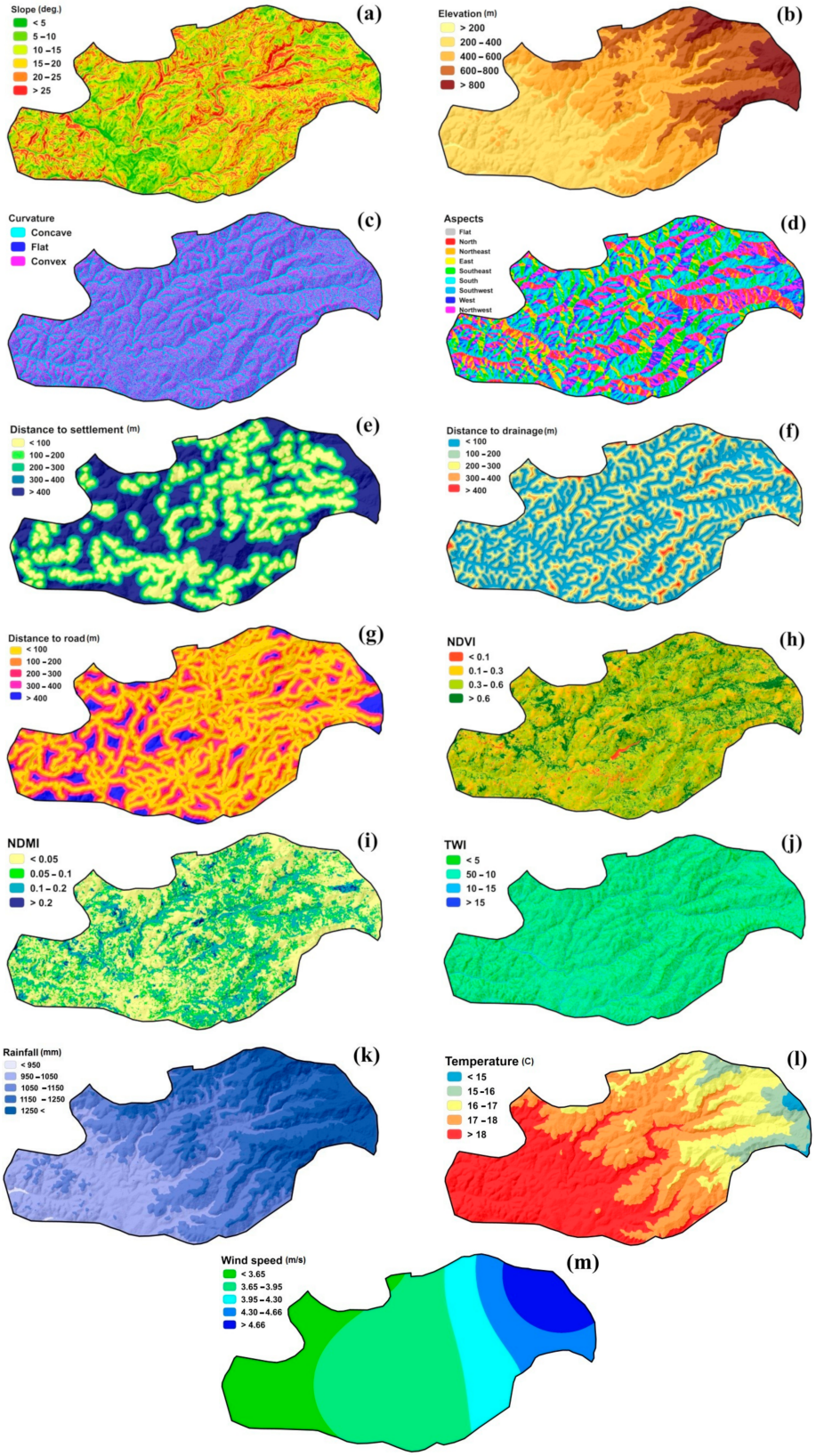

Figure 3. Forest fire-triggering factors: (**a**) slope, (**b**) aspect, (**c**) curvature, (**d**) elevation, (**e**) distance to settlement, (**f**) distance to drainage, (**g**) distance to road, (**h**) NDVI, (**i**) NDMI, (**j**) TWI, (**k**) rainfall, (**l**) temperature and (**m**) wind speed.

2.4.4. Aspects (AS)

The slope aspect factor sets the micro-climatic condition of the slope, including the amount of solar radiation absorbed, the temperature of the slope sheet, the abundance of moisture, wind flow, and the extent of development of the vegetation system [43,44]. In the northern hemisphere, the south and west slope aspects receive the maximum possible solar radiation calories, unlike the northern aspects [45]. Slope aspects of the study area were classified into nine orientations (Figure 3d): Flat, North, Northeast, East, Southeast, South, Southwest, West, and Northwest.

2.4.5. Distance to Settlement (DS)

Distance to settlement is one of the most influential human spatial indicators that reflect the intensity of human pressure on forest ecosystems [41]. In this regard, forest dwellers can cause accidental or non-accidental fires in dry seasons as a result of cooking, cigar butts, and coaling [46]. The Euclidean distance from the settlement map was divided into five classes (Figure 3e): <100, 100–200, 200–300, 300–400, and >400 m.

2.4.6. Distance to Drainage (DD)

Distance to the drainage network leads to the development of a fire-retardant zone, reducing the fire intensity and encircling the firing range [47,48]. The study area is characterized by a rich and mature network of seasonal runoff streams. The Euclidean distance from the drainage map was divided into five classes (Figure 3f): <100, 100–200, 200–300, 300–400, and >400 m.

2.4.7. Distance to Road (DR)

A road network is one of the most important infrastructure foundations in the framework of forest management and investment [49]. Moreover, a road network develops a field of direct contact between intensive human activities and the forest system, and thus, leads to the formation of a surrounding spatial zone that increases the possibility of forest fire events. The construction of a road network, excavations, the removal of vegetation cover, and the movement of travelers and visitors are among the triggers for fires along a forest road network [50]. With an interval of 100 m, the Euclidean distance from the road map was divided into five classes (Figure 3g): <100, 100–200, 200–300, 300–400, and <400 m.

2.4.8. Normalized Difference Vegetation Index (NDVI)

Exploring the spatial distribution of vegetation density provides an accurate visual interpretation of the intensity and extent of the forest fire. The NDVI reflects the plant photosynthesis process—consequently, the soil and plant water content, which affects the possibility of forest fire propagation [51,52]. As noted in Figure 3h, the NDVI value map was classified within four levels: <0.1, 0.1–0.3, 0.3–0.6, and >0.6.

2.4.9. Normalized Difference Moisture Index (NDMI)

Several studies indicate a strong positive correlation between plant and soil moisture and the spread of fires in terms of plant water stress [53]. Moreover, the soil humidity has a stronger effect than the dominant weather characteristics on the occurrence of forest fires. The NDMI, which evaluates plant water stress, is one of the most widely used indicators in fire susceptibility studies [54]. The abundance of plant moisture is distinguished using the NDMI according to the color intensity that reflects higher humidity (values higher than 1) and vice versa. Figure 3i shows the spatial distribution of NDMI values after classifying them into four categories: <0.05, 0.05–0.1, 0.1–0.2, and >0.2.

2.4.10. Topographic Wetness Index (TWI)

The potential of a forest fire and its propagation increases with a decrease in the topographical moisture and an increase in the water need to saturate the terrain [40,55]. The TWI reflects the abundance of surface moisture, thus controlling the spatial evolution

of the spread of forest fire [6,56,57]. Figure 3j depicts the classification of spatial distribution of TWI values: <5, 5–10, 10–15, and >15.

2.4.11. Rainfall (RF)

Rainfall is a critical climatic parameter in the spread of forest fires. Rainfall plays an important role in the variability of fuel moisture abundance and surface saturation [58,59]. The prospect of forest fires increases as precipitation decreases, and vice versa [60]. The spatial distribution of rainfall in the Al-Draikich area was derived based on the rainfall data from 1990–2020 obtained from the General Directorate of Meteorology, Damascus. Figure 3k illustrates the classification of the spatial distribution of rainfall values: <950, 950–1050, 1050–1150, 1150–1250, and >1250 mm.

2.4.12. Temperature (TM)

Similar to precipitation, an increase in temperature represents an influential climatic factor in terms of the increase in the occurrence and forest fires [39]. Many scholars of fire risk point to the direct spatial relationship between temperature and forest fires [32]. In this regard, rising temperatures make forest systems more vulnerable to fires due to lower moisture content. In the study area, the period from June to November passes with high suitability for forest fire frequency [61]. The spatial distribution of temperature in the Al-Draikich area was derived based on the rainfall data from 1990–2020 obtained from the General Directorate of Meteorology, Damascus. Figure 3l shows the classification of the spatial distribution of temperature values: <15 °C, 15–16 °C, 16–17 °C, 17–18 °C, and >18 °C.

2.4.13. Wind Speed (WS)

The wind speed has a strong effect on forest fire incidents because it reduces the abundance of plants and the topographic and soil moisture [62]. In this context, the role of wind speed increases in the effectiveness of forest fire propagation during the dry season [63]. The spatial distribution of rainfall in the Al-Draikich area was derived on the basis of the wind speed data from 1990–2020 obtained from the General Directorate of Meteorology, Damascus. Figure 3m illustrates the classification of the spatial distribution of wind speed values: <3.65, 3.65–3.95, 3.95–4.30, 4.30–4.66, and >4.66 m/s.

2.5. Statistical Analyses

Statistical analysis is considered the most critical step in mapping forest fire sensitivity because this analysis determines the weights (i.e., importance) of the different classes of a given factor on forest fire occurrence. The frequency ratio (FR) and the analytic hierarchy process (AHP) are considered among the most widely used statistical methods that produce reliable outputs [21,23,58]. Thus, forest fire susceptibility in the study area was analyzed based on the FR and AHP methods, which are described in the following subsections.

2.5.1. Frequency Ratio (FR)

The FR method is one of the most widely used bivariate methods for mapping spatial targeting to the occurrence of natural hazards, including forest fires [2,11,64]. The principle of the FR method is to estimate the probability of recurring current risk events in the future in proportional linking with the current geographical characteristics representing the driving forest fire factors [65,66]. If the FR value is higher than 1, it indicates a significant impact of the classification of the driving criterion on increasing the susceptibility of a future forest fire event, and vice versa if it is less than 1. The *FR* calculated by using Equation (4):

$$FR = \frac{S/M}{Q/R} \quad (4)$$

where S determines the number of forest fire events for each class of each motivated parameter, M determines the overall forest fire events, Q defines the number of pixels for each class of the criterion, and R determines the total number of pixels.

2.5.2. Analytic Hierarchy Process (AHP)

The AHP method is among the most widely applied methods globally with reliable results to assess the spatial susceptibility of natural hazards, including forest fires [1,21,23,58,67]. In the current study, the AHP method was used to produce the forest fire susceptibility map. The hierarchical topographical, climatic, environmental, and anthropogenic criteria were organized for a pair-wise comparison process [68,69]. According to Table 2, the relative weightage of each individual criterion was determined by calibrating the effect intensity of each criterion in relation to the other criteria in enhancing forest fire susceptibility.

Table 2. The fundamentals scale of absolute numbers for AHP.

Intensity of Importance	Definition	Explanation
1	Equal importance	Two activities contribute equally to the objective.
2	Weak or slight	
3	Moderate importance	Experience and judgment slightly favor one activity over another.
4	Moderate plus	
5	Strong importance	Experience and judgment strongly favor one activity over another.
6	Strong plus	
7	Very strong or demonstrated importance	An activity is favored very strongly over another; its dominance is demonstrated in practice.
8	Very, very strong	
9	Extreme importance	The evidence favoring one activity over another is of the highest possible order of affirmation.
Reciprocals	Opposites	Used for inverse comparison.

Experts' opinions, extensive field study, an understanding of the driving factors, and the characteristics of the study area were among the rules that were taken into consideration when determining the relative weightage of each individual criterion. The experts' team (14 experts) was formed from the General Authority for Remote Sensing in Damascus and the Biodiversity Division in the Directorate of Agriculture in Tartous, Syria. These pair-wise comparisons enable the development of a pair-wise comparison matrix that assesses the susceptibility of each criterion in forest fire susceptibility (Equation (5)):

$$\begin{array}{c} C1 \\ C2 \\ C3 \\ . \\ . \\ . \\ Cn \end{array} \begin{pmatrix} \mathrm{Ps1}/Ps2 & Ps1/Ps2 & \ldots & Ps1/Psn \\ Ps2/Ps1 & Ps2/Ps2 & \ldots & Ps2/Psn \\ Ps3/Ps1 & Ps3/Ps2 & \ldots & Ps3/Psn \\ . & . & & . \\ . & . & & . \\ . & . & & . \\ Psn/Ps1 & Psn/Ps2 & \ldots & Psn/Psn \end{pmatrix} \quad (5)$$

where C is the selected criteria and Ps is the priority score given to each criterion. After determining the final weights for each criterion, it is important to carry out a process of consistency evaluation of the experts' suggestions (Equation (6)):

$$CR = \frac{CI}{RI} \quad (6)$$

where CR is the consistency ratio (CR is utilized to specify the value of likelihood), CI is the consistency index (CI relies on the order of the matrix specified by Saaty [70]), and RI

is the random index (random inconsistency) (Table 3). *CI* is measured with the following equation (Equation (7)):

$$CI = \lambda_{max} - n/(n - 1) \quad (7)$$

where, *CI* is the consistency index, λ is the consistency vector (greatest or principal eigenvalue of the matrix), and n refers to the number of total criteria.

Table 3. The random inconsistency values.

Number of Criteria	1	2	3	4	5	6	7	8	9	10	11	12	13	14
Random Inconsistency	0.00	0.00	0.58	0.90	1.12	1.24	1.32	1.41	1.45	1.49	1.51	1.54	1.56	1.57

2.6. Accuracy Assessment of Forest Fire Susceptibility Maps

Validation is an essential procedure in forest fire susceptibility assessment for specifying the predictive performance of these selected methods [6,9,53]. The receiver operating characteristic–area under the curve (ROC–AUC) is a widely used method for evaluating the accuracy of utilized models, and it is commonly used in forest fire hazard-mapping studies due to its flexibility of explanation of degree susceptibility studies [71,72]. The ROC curve is a graphic method for testing the trade-off between specificity and sensitivity, with the *x*-axis illustrating a false-positive rate (specificity—1) and the *y*-axis displaying a true-positive rate (sensitivity) in order to assess the quality of the model's forecasting ability [64,73–76].

3. Results

3.1. Forest Fire Susceptibility Mapping

3.1.1. Forest Fire Susceptibility Mapping with the FR Method

Using the logic of relative calibration between the specific forest fire events as training points and as a set of driving factors, or the FR method, a forest fire susceptibility map was produced in the study area. Table 4 presents the result of applying the FR index of forest fire training events for each causative sub-factor. By using the *Raster Calculator* tool in the GIS environment, a map of forest fire susceptibility was produced and classified using the *Natural Breaks* tool as very low (12%), low (26.07%), moderate (28.27%), high (21.85%), and very high (11.82%) (Figure 4).

Table 4. The spatial association between the classes of causative factors and current forest fire sites extracted from the FR.

No.	Factor	Class	No. of Forest Fires	% of Forest Fires	No. of Pixels in Domain	% of Domain	FR
1	Slope (SL) (deg.)	<5	1	4.55	78,901	6.61	0.69
		5–10	2	9.09	225,232	18.87	0.48
		10–15	7	31.82	311,353	26.09	1.22
		15–20	5	22.73	313,773	26.29	0.86
		20–25	4	18.18	172,842	14.48	1.26
		>25	3	13.64	91,244	7.65	1.78
2	Elevation (El) (m)	<200	0	0	2244	0.19	0
		200–400	5	22.73	386,567	32.39	0.7
		400–600	12	54.55	432,655	36.26	1.5
		600–800	4	18.18	265,559	22.25	0.82
		>800	1	4.55	106,320	8.91	0.51
3	Curvature (CV)	Concave	7	31.82	449,983	37.71	0.84
		Flat	4	18.18	290,548	24.35	0.75
		Convex	11	50	452,814	37.94	1.32

Table 4. *Cont.*

No.	Factor	Class	No. of Forest Fires	% of Forest Fires	No. of Pixels in Domain	% of Domain	FR
4	Aspects (AS)	Flat	0	0	2430	0.2	0
		North	0	0	62,626	5.25	0
		Northeast	1	4.55	67,936	5.69	0.18
		East	3	13.64	91,840	7.7	0.39
		Southeast	7	31.82	179,250	15.02	0.47
		South	3	13.64	216,539	18.15	0.17
		Southwest	5	22.73	174,690	14.64	0.34
		West	1	4.55	153,288	12.85	0.08
		Northwest	2	9.09	172,575	14.46	0.14
		North	0	0	72,171	6.05	0
5	Distance to settlement (DS) (m)	<100	4	18.18	314,685	26.37	0.69
		100–200	5	22.73	203,579	17.06	1.33
		200–300	7	31.82	174,913	14.66	2.17
		300–400	5	22.73	140,437	11.77	1.93
		>400	1	4.55	359,731	30.14	0.15
6	Distance to drainage (DD) (m)	<100	12	54.55	515,300	43.18	1.26
		100–200	8	36.36	400,678	33.58	1.08
		200–300	2	9.09	218,759	18.33	0.5
		300–400	0	0	51,924	4.35	0
		>400	0	0	6684	0.56	0
7	Distance to road (DR) (m)	<100	8	36.36	584,659	48.99	0.74
		100–200	10	45.45	313,772	26.29	1.73
		200–300	2	9.09	152,051	12.74	0.71
		300–400	1	4.55	74,051	6.21	0.73
		>400	1	4.55	68,812	5.77	0.79
8	NDVI	<0.1	1	4.55	17,383	1.46	3.12
		0.1–0.3	3	13.64	264,964	22.2	0.61
		0.3–0.6	15	68.18	688,852	57.72	1.18
		>0.6	3	13.64	222,146	18.62	0.73
9	NDMI	<0.05	13	59.09	605,701	50.76	1.16
		0.05–0.1	5	22.73	316,206	26.5	0.86
		0.1–0.2	4	18.18	254,833	21.35	0.85
		>0.2	0	0	16,605	1.39	0
10	Topographic Wetness Index (TWI)	<5	8	36.36	387,855	32.5	1.12
		5–10	13	59.09	771,304	64.63	0.91
		10–15	1	4.55	28,410	2.38	1.91
		>15	0	0	5776	0.48	0
11	Rainfall (RF) (mm)	<950	0	0	2244	0.19	0
		950–1050	3	13.64	314,981	26.39	0.52
		1050–1150	15	68.18	388,447	32.55	2.09
		1150–1250	2	9.09	292,709	24.53	0.37
		>1250	2	9.09	194,964	16.34	0.56
12	Temperature (TM) (°C)	<15	7	31.82	482,874	40.46	0.79
		15–16	11	50	391,289	32.79	1.52
		16–17	4	18.18	226,069	18.94	0.96
		17–18	0	0	81,499	6.83	0
		>18	0	0	11,614	0.97	0
13	Wind speed (WS) (m/s)	<3.65	2	9.09	243,083	20.37	0.45
		3.65–3.95	14	63.64	543,309	45.53	1.4
		3.95–4.30	4	18.18	173,464	14.54	1.25
		4.30–4.66	1	4.55	130,006	10.89	0.42
		>4.66	1	4.55	103,483	8.67	0.52

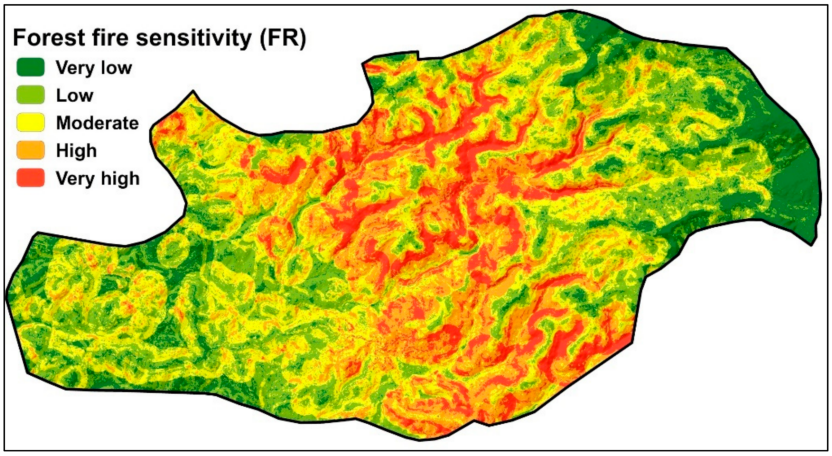

Figure 4. Forest fire susceptibility map produced using the FR method.

3.1.2. Forest Fire Susceptibility Mapping with the AHP Method

Based on a number of considerations, especially the opinions of experts, a pair-wise comparison matrix was developed that evaluates the effect of each factor in enhancing the probability of forest fires compared to another factor, with the final weights as shown in Tables 5–7, which also illustrate the scores of the factor classes. It was necessary to examine the consistency of expert opinions for 13 driving factors.

Table 5. Pair-wise comparison matrix by AHP.

Factors	SL	EL	CR	AS	DS	DD	DR	NDVI	NDMI	TWI	RF	TM	WS
Slope (SL)	1	5.00	7.00	5.00	6.00	6.00	5.00	4.00	3.00	6.00	5.00	6.00	3.00
Elevation (El)	0.20	1	2.00	3.00	2.00	5.00	4.00	4.00	3.00	5.00	3.00	5.00	3.00
Curvature (CV)	0.14	0.50	1	3.00	2.00	3.00	4.00	3.00	2.00	3.00	4.00	3.00	2.00
Aspects (AS)	0.20	0.33	0.33	1	1.00	3.00	2.00	4.00	3.00	4.00	2.00	3.00	2.00
Distance to settlement (DS)	0.17	0.50	0.50	1.00	1	2.00	1.00	2.00	4.00	3.00	2.00	4.00	2.00
Distance to drainage (DD)	0.17	0.20	0.33	0.33	0.50	1	1.00	2.00	1.00	2.00	2.00	4.00	1.00
Distance to road (DR)	0.20	0.25	0.25	0.50	1.00	1.00	1	2.00	2.00	3.00	4.00	3.00	2.00
NDVI	0.25	0.25	0.33	0.25	0.50	0.50	0.50	1	1.00	2.00	1.00	3.00	1.00
NDMI	0.33	0.33	0.50	0.33	0.25	1.00	0.50	1.00	1	2.00	1.00	2.00	1.00
Topographic Wetness Index (TWI)	0.17	0.20	0.33	0.25	0.33	0.50	0.33	0.50	0.50	1	1.00	2.00	1.00
Rainfall (RF)	0.20	0.33	0.25	0.50	0.50	0.50	0.25	1.00	1.00	1.00	1	3.00	2.00
Temperature (TM)	0.17	0.20	0.33	0.33	0.25	0.25	0.33	0.33	0.50	0.50	0.33	1	1.00
Wind speed (WS)	0.33	0.33	0.50	0.50	0.50	1.00	0.50	1.00	1.00	1.00	0.50	1.00	1

The CR value was 6.25%, which is less than 10%, indicating that the judgments were consistent and could be used for mapping the forest fire susceptibility. In addition, Table 6 shows the proposed weights of the factors' classes. In this context, it can be noted that the slope and elevation factors were among the most influential factors for predicting forest fires in the study area. This can be explained by the strong association of the extreme spatial variability of the other factors with slope and elevation, which increase the susceptibility of forest fires. Using the *Reclassify* and *Weighted Sum* tools, all the trigging factor layers were combined to produce a forest fire susceptibility map in the study area, which was classified using the *Natural Breaks* method as very low (15.83%), low (17.91%), moderate (34.75%), high (21.79%), and very high (9.73%) (Figure 5).

Table 6. Normalized pair-wise comparison matrix and computation of factor weights.

	SL	EL	CR	AS	DS	DD	DR	NDVI	NDMI	TWI	RF	TM	WS	Weight	Rank
SL	0.283	0.531	0.513	0.313	0.379	0.242	0.245	0.155	0.130	0.179	0.186	0.150	0.136	0.265	1
El	0.057	0.106	0.147	0.188	0.126	0.202	0.196	0.155	0.130	0.149	0.112	0.125	0.136	0.141	2
CV	0.040	0.053	0.073	0.188	0.126	0.121	0.196	0.116	0.087	0.090	0.149	0.075	0.091	0.108	3
AS	0.057	0.035	0.024	0.063	0.063	0.121	0.098	0.155	0.130	0.119	0.075	0.075	0.091	0.085	4
DS	0.048	0.053	0.037	0.063	0.063	0.081	0.049	0.077	0.174	0.090	0.075	0.100	0.091	0.077	5
DD	0.048	0.021	0.024	0.021	0.032	0.040	0.049	0.077	0.043	0.060	0.075	0.100	0.045	0.049	7
DR	0.057	0.027	0.018	0.031	0.063	0.040	0.049	0.077	0.087	0.090	0.149	0.075	0.091	0.066	6
NDVI	0.071	0.027	0.024	0.016	0.032	0.020	0.024	0.039	0.043	0.060	0.037	0.075	0.045	0.039	10
NDMI	0.093	0.035	0.037	0.021	0.016	0.040	0.024	0.039	0.043	0.060	0.037	0.050	0.045	0.042	8
TWI	0.048	0.021	0.024	0.016	0.021	0.020	0.016	0.019	0.022	0.030	0.037	0.050	0.045	0.028	12
RF	0.057	0.035	0.018	0.031	0.032	0.020	0.012	0.039	0.043	0.030	0.037	0.075	0.091	0.040	9
TM	0.048	0.021	0.024	0.021	0.016	0.010	0.016	0.013	0.022	0.015	0.012	0.025	0.045	0.022	13
WS	0.093	0.035	0.037	0.031	0.032	0.040	0.024	0.039	0.043	0.030	0.019	0.025	0.045	0.038	11
λ	14.17														
n	13														
CI	0.097														
RI: n = 13	1.56														
CR	0.062														
CR%	6.25														

λ: Maximum eigenvalue, *CI*: consistency index, *CR*: consistency ratio.

Table 7. Weights of the criteria and scores of the sub-criteria.

No.	Factor	Sub-Criteria	Susceptibility Class of FRS	Rating	AHP Weight
1	Slope (SL) (deg.)	<5	Very low	1	0.265
		5–10	Low	2	
		10–15	Moderate	3	
		15–20	High	4	
		20–25	Very high	5	
		>25	Very high	5	
2	Elevation (El) (m)	<200	Very high	5	0.141
		200–400	High	4	
		400–600	Moderate	3	
		600–800	Low	2	
		>800	Very low	1	
3	Curvature (CV)	Concave	Moderate	3	0.108
		Flat	Very high	5	
		Convex	High	4	
4	Aspects (AS)	Flat	Very high	5	0.085
		North	Moderate	3	
		Northeast	Low	2	
		East	Very high	5	
		Southeast	Very high	5	
		South	High	4	
		Southwest	High	4	
		West	Very high	5	
		Northwest	Moderate	3	
		North	Low	2	

Table 7. *Cont.*

No.	Factor	Sub-Criteria	Susceptibility Class of FRS	Rating	AHP Weight
5	Distance to settlement (DS) (m)	<100	Very high	5	0.077
		100–200	High	4	
		200–300	Moderate	3	
		300–400	Low	2	
		>400	Very low	1	
6	Distance to drainage (DD) (m)	<100	Very high	5	0.049
		100–200	High	4	
		200–300	Moderate	3	
		300–400	Low	2	
		>400	Very low	1	
7	Distance to road (DR) (m)	<100	Very high	5	0.066
		100–200	High	4	
		200–300	Moderate	3	
		300–400	Low	2	
		>400	Very low	1	
8	NDVI	<0.1	Low	2	0.039
		0.1–0.3	Moderate	3	
		0.3–0.6	High	4	
		>0.6	Very high	5	
9	NDMI	<0.05	Low	1	0.042
		0.05–0.1	Moderate	3	
		0.1–0.2	High	4	
		>0.2	Very high	5	
10	Topographic Wetness Index (TWI)	<5	Low	2	0.028
		5–10	Moderate	3	
		10–15	High	4	
		>15	Very high	5	
11	Rainfall (RF) (mm)	<950	Very high	5	0.04
		950–1050	High	4	
		1050–1150	Moderate	3	
		1150–1250	Low	2	
		<1250	Very low	1	
12	Temperature (TM) (°C)	<15	Very low	1	0.022
		15–16	Low	2	
		16–17	Moderate	3	
		17–18	High	4	
		>18	Very high	5	
13	Wind speed (WS) (m/s)	<3.65	Very low	1	0.038
		3.65–3.95	Low	2	
		3.9–4.30	Moderate	3	
		4.30–4.66	High	4	
		>4.66	Very high	5	

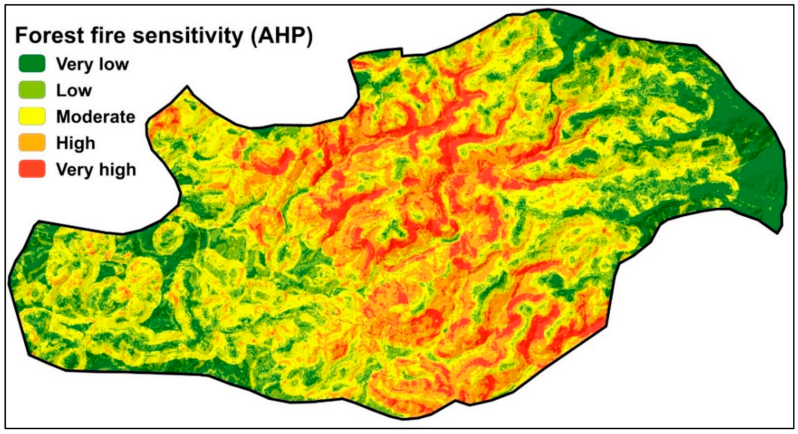

Figure 5. Forest fire susceptibility map utilizing the AHP method.

3.2. Validation

Evaluating the accuracy of prediction outputs is a critical and complementary measure to achieve the maximum benefit of modeling studies. In the current analysis, ROC–AUC was used to test the accuracy of the produced forest fire susceptibility maps. The results showed that the FR method achieved the highest accuracy of spatial prediction, followed by the AHP method, with AUC values of 0.864 and 0.838, respectively (Figure 6). Although the FR method achieved the best accuracy in producing a map of forest fire susceptibility in the study area, it did not prevent the AHP method from producing an objective and constructive susceptibility map.

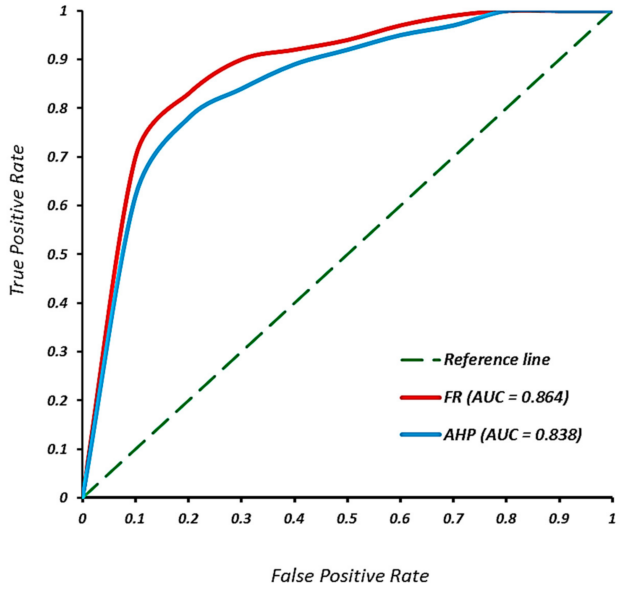

Figure 6. ROC plots for FR and AHP.

4. Discussion

The environmental threats posed by forest fires to ecological sustainability and the biodiversity of ecosystems are increasing globally, especially in light of climate change and rapid population growth. In this regard, the need to determine the spatial susceptibility of forest fires has become crucial in the context of integrated management of global forest wealth. In this study, a comprehensive spatial assessment of the potential susceptibility of forest fires in the Al-Draikich area was conducted using a combination of FR/AHP and GIS/RS techniques. These final spatial outputs allowed the grading of the spatial distribution of potential forest fire susceptibility in the study area (Table 8) based on five categories: very low, low, moderate, high, and very high.

Table 8. Spatial classes of forest hazard susceptibility utilizing the FR and AHP methods.

Degree	Forest Fire Susceptibility	FR		AHP	
		Area (km^2)	%	Area (km^2)	%
1	Very low	22.32	12.00	29.46	15.83
2	Low	48.51	26.07	33.33	17.91
3	Moderate	52.61	28.27	64.66	34.75
4	High	40.65	21.85	40.54	21.79
5	Very high	21.99	11.82	18.10	9.73

The produced maps indicate that high and very high spatial distribution of fire susceptibility could be observed in the slopes of the central, northern, and northeastern regions of the study area. In the analysis, these areas were characterized by a combination of different factors that can promote forest fires, especially steep slopes, high elevation, dense forest

cover, fuel heating, moisture, high wind velocity, and proximity to settlements and road networks. These results are consistent with the various forest fire susceptibility studies worldwide [1,2,4,21,25,66,77]. In this context, the mapping process for forest fire susceptibility based on the FR and AHP methods showed high flexibility and reliability. ROC with AUC provided satisfactory evidence of the quality of the outputs of this study.

Moreover, the application of the FR and AHP methods provided a rich evaluation that enables a comparison of the obtained spatial outcomes. The FR method involves conducting a spatial association analysis between fire events and the driving factors, whereas the AHP method provides a spatial analysis of the views of a selected number of experts on the spatial variability of forest fire sensitivity. Nevertheless, the FR method was more accurate in deriving a fire susceptibility map than the AHP method. Similar results were reported in related studies [78]. However, the forest fire susceptibility literature shows a high objective reliability in deriving maps using FR and AHP, such as in Turkey [79], Ethiopia [80], and Brazil [81]. In the context of explaining the higher accuracy of the FR method than that of the AHP method, it needs to be stated that the FR method took into account the true spatial distribution of forest fire events in relation to sub-classifications of the driving factors, thus determining the effectiveness of each sub-classification's influence in enhancing the probability of forest fires. On the other hand, the AHP method, in determining the final weights of the causative factors, was based on expert opinions with varying consistency factors.

The present assessment shows the spatial behavior of the future development of forest fires that will threaten the remnants of degraded forest cover in the study area. In this setting, these fires will constitute an additional factor enhancing the loss of forest cover under the current war conditions in the country. Moreover, the patterns of indiscriminate exploitation of forest wealth will increase the probability of forest fires in the study area through negative friction between forests and humans [80]. In detail, the current war conditions in the country have led to a severe shortage of fossil energy resources, with almost a complete disruption of electrical power over the past decade [81]. Thus, the locals have resorted to forest resources to find alternative energy for heating, cooking, and lighting. Moreover, the deteriorating economic conditions have led some residents to resort to charcoal production to ensure financial support [82,83]. In the case of the study area, charcoal production is carried out in a traditional way, causing huge fires within the forests that often go out of control. However, investigations carried out by local authorities showed that charring was one of the most significant causes of forest fires during 2019, 2020, and 2021. These results were reported in studies conducted by [7,26].

The fieldwork provided evidence of the spatial output reliability presented in this study, especially areas with high and very high susceptibility to forest fires. These areas included the most dangerous incidents of forest fires in terms of spread and catastrophic consequences, especially the villages of *Dahr*, *Genena Raslan*, *Al-Afsunah*, and *Ain Hajja*.

The final outputs of this study provided a reliable spatial basis within the framework of managing and maintaining the sustainability of the forest system in the study area. Areas of high and very high forest fire susceptibility must be targeted with a set of measures—for example, establishing an early fire-warning system, constructing watchtowers, or facilitating access through the construction and maintenance of off-roads. In addition, the guarding system must be improved by activating the forestry control and patrolling systems. Friction between humans and the forest must also be reduced as much as possible through the establishment of reserves with administrative control.

5. Conclusions

Forest fires are one of the most significant manifestations of global forest system degradation. The aim of this evaluation was to target the spatial susceptibility of forest fires in the western region of Syria (Al-Draikish region), which is frequently exposed to forest fire incidents. The integration of field surveys, remote sensing and GIS techniques, and related statistical analyses (FR and AHP methods) were used to produce two forest

fire susceptibility maps in a flexible and effective manner. The results of the current study reported that the factors of topography, climate, moisture, plant diversity, and random urbanization were among the factors that stimulate the susceptibility of forest fires in the study area. Moreover, the results of mapping accuracy assessment indicate that the selection of individual driving factors was satisfactory, taking into account the specificity of the study area and the relevant literature. In addition, the resulting forest susceptibility map using FR was found to be more accurate than the AHP method. The results of this study enhance the ability of forest planners and managers in the study area to improve forest protection and prevention services.

Author Contributions: Conceptualization, H.G.A. and H.A.; methodology, M.A.-M., H.G.A. and A.A.A.D.; software, A.A.A.D. and H.G.A.; validation, M.A.-M.; formal analysis, H.G.A., H.A., A.A.A.D. and M.A.-M.; investigation, H.G.A. and A.A.A.D.; resources, M.A.-M.; data curation, H.G.A.; writing—original draft preparation, H.G.A., H.A., A.A.A.D. and M.A.-M.; writing—review and editing, M.A.-M., H.A., A.A.A.D. and H.G.A.; visualization, H.G.A. and A.A.A.D.; supervision and project administration, H.A.; funding acquisition, H.A. All authors have read and agreed to the published version of the manuscript.

Funding: This project was funded by Princess Nourah bint Abdulrahman University Research Supporting Project Number PNURSP2022R241, Princess Nourah bint Abdulrahman University, Riyadh, Saudi Arabia. The article processing charge was funded by the Deanship of Scientific Research, Qassim University.

Institutional Review Board Statement: Not applicable.

Informed Consent Statement: Not applicable.

Data Availability Statement: Not applicable.

Acknowledgments: The authors would like to thank Princess Nourah bint Abdulrahman University for supporting the project and the Deanship of Scientific Research, Qassim University, for funding the publication of this project.

Conflicts of Interest: The authors declare no conflict of interest.

References

1. Abedi Gheshlaghi, H.; Feizizadeh, B.; Blaschke, T. GIS-based forest fire risk mapping using the analytical network process and fuzzy logic. *J. Environ. Plan. Manag.* **2020**, *63*, 481–499. [CrossRef]
2. Tuyen, T.T.; Jaafari, A.; Yen, H.P.H.; Nguyen-Thoi, T.; Van Phong, T.; Nguyen, H.D.; Van Le, H.; Phuong, T.T.M.; Nguyen, S.H.; Prakash, I. Mapping forest fire susceptibility using spatially explicit ensemble models based on the locally weighted learning algorithm. *Ecol. Inform.* **2021**, *63*, 101292. [CrossRef]
3. Mafi-Gholami, D.; Jaafari, A.; Zenner, E.K.; Kamari, A.N.; Bui, D.T. Spatial modeling of exposure of mangrove ecosystems to multiple environmental hazards. *Sci. Total Environ.* **2020**, *740*, 140167. [CrossRef] [PubMed]
4. Nuthammachot, N.; Stratoulias, D. A GIS-and AHP-based approach to map fire risk: A case study of Kuan Kreng peat swamp forest, Thailand. *Geocarto Int.* **2021**, *36*, 212–225. [CrossRef]
5. McGuire, S.; IFAD; WFP. *The State of Food Insecurity in the World 2015: Meeting the 2015 International Hunger Targets: Taking Stock of Uneven Progress*; FAO: Rome, Italy, 2015; pp. 623–624.
6. Jaafari, A.; Mafi-Gholami, D.; Pham, B.T.; Tien Bui, D. Wildfire probability mapping: Bivariate vs. multivariate statistics. *Remote Sens.* **2019**, *11*, 618. [CrossRef]
7. Abdo, H.G. Impacts of war in Syria on vegetation dynamics and erosion risks in Safita area, Tartous, Syria. *Reg. Environ. Chang.* **2018**, *18*, 1707–1719. [CrossRef]
8. Novo, A.; Fariñas-Álvarez, N.; Martínez-Sánchez, J.; González-Jorge, H.; Fernández-Alonso, J.M.; Lorenzo, H. Mapping forest fire risk—A case study in Galicia (Spain). *Remote Sens.* **2020**, *12*, 3705. [CrossRef]
9. Pham, B.T.; Jaafari, A.; Avand, M.; Al-Ansari, N.; Dinh Du, T.; Yen, H.P.H.; Phong, T.V.; Nguyen, D.H.; Le, H.V.; Mafi-Gholami, D. Performance evaluation of machine learning methods for forest fire modeling and prediction. *Symmetry* **2020**, *12*, 1022. [CrossRef]
10. Hong, H.; Jaafari, A.; Zenner, E.K. Predicting spatial patterns of wildfire susceptibility in the Huichang County, China: An integrated model to analysis of landscape indicators. *Ecol. Indic.* **2019**, *101*, 878–891. [CrossRef]
11. Jaafari, A.; Razavi Termeh, S.V.; Bui, D.T. Genetic and firefly metaheuristic algorithms for an optimized neuro-fuzzy prediction modeling of wildfire probability. *J. Environ. Manag.* **2019**, *243*, 358–369. [CrossRef]
12. Santín, C.; Doerr, S.H. Fire effects on soils: The human dimension. *Philos. Trans. R. Soc. B Biol. Sci.* **2016**, *371*, 20150171. [CrossRef] [PubMed]

13. Gupta, S.; Roy, A.; Bhavsar, D.; Kala, R.; Singh, S.; Kumar, A.S. Forest fire burnt area assessment in the biodiversity rich regions using geospatial technology: Uttarakhand Forest Fire event 2016. *J. Indian Soc. Remote Sens.* **2018**, *46*, 945–955. [CrossRef]
14. Venkatesh, K.; Preethi, K.; Ramesh, H. Evaluating the effects of forest fire on water balance using fire susceptibility maps. *Ecol. Indic.* **2020**, *110*, 105856. [CrossRef]
15. Ibrahem, A.; Koubaily, E.; Thabeet, A. Modeling the natural regeneration of Cedrus libani A. Richard in Slenfeh, Syria, using binary logistic regression. *Model. Earth Syst. Environ.* **2021**, *7*, 41–55. [CrossRef]
16. Recanatesi, F.; Giuliani, C.; Ripa, M.N. Monitoring Mediterranean Oak decline in a peri-urban protected area using the NDVI and Sentinel-2 images: The case study of Castelporziano State Natural Reserve. *Sustainability* **2018**, *10*, 3308. [CrossRef]
17. Almohamad, H.; Knaack, A.L.; Habib, B.M. Assessing spatial equity and accessibility of public green spaces in Aleppo City, Syria. *Forests* **2018**, *9*, 706. [CrossRef]
18. Verkerk, P.J.; Fitzgerald, J.B.; Datta, P.; Dees, M.; Hengeveld, G.M.; Lindner, M.; Zudin, S. Spatial distribution of the potential forest biomass availability in Europe. *For. Ecosyst.* **2019**, *6*, 5. [CrossRef]
19. Çolak, E.; Sunar, F. Evaluation of forest fire risk in the Mediterranean Turkish forests: A case study of Menderes region, Izmir. *Int. J. Disaster Risk Reduct.* **2020**, *45*, 101479. [CrossRef]
20. Liu, B.; Spiekermann, R.; Zhao, C.; Püttmann, W.; Sun, Y.; Jasper, A.; Uhl, D. Evidence for the repeated occurrence of wildfires in an upper Pliocene lignite deposit from Yunnan, SW China. *Int. J. Coal Geol.* **2022**, *250*, 103924. [CrossRef]
21. Busico, G.; Giuditta, E.; Kazakis, N.; Colombani, N. A hybrid GIS and AHP approach for modelling actual and future forest fire risk under climate change accounting water resources attenuation role. *Sustainability* **2019**, *11*, 7166. [CrossRef]
22. Arca, D.; Hacısalihoğlu, M.; Kutoğlu, Ş.H. Producing forest fire susceptibility map via multi-criteria decision analysis and frequency ratio methods. *Nat. Hazards* **2020**, *104*, 73–89. [CrossRef]
23. Akbulak, C.; Tatlı, H.; Aygün, G.; Sağlam, B. Forest fire risk analysis via integration of GIS, RS and AHP: The Case of Çanakkale, Turkey. *J. Hum. Sci.* **2018**, *15*, 2127–2143. [CrossRef]
24. Mohamed, M.A. An Assessment of Forest Cover Change and Its Driving Forces in the Syrian Coastal Region during a Period of Conflict, 2010 to 2020. *Land* **2021**, *10*, 191. [CrossRef]
25. Almohamad, H. Impact of land cover change due to armed conflicts on soil erosion in the basin of the northern Al-Kabeer River in Syria using the RUSLE model. *Water* **2020**, *12*, 3323. [CrossRef]
26. Schon, J.; Mezuman, K.; Heslin, A.; Field, R.D.; Puma, M.J. How fire patterns reveal uneven stabilization at the end of conflict: Examining Syria's unusual fire year in 2019. *Environ. Res. Lett.* **2021**, *16*, 044046. [CrossRef]
27. Abdo, H.G. Evolving a total-evaluation map of flash flood hazard for hydro-prioritization based on geohydromorphometric parameters and GIS–RS manner in Al-Hussain river basin, Tartous, Syria. *Nat. Hazards* **2020**, *104*, 681–703. [CrossRef]
28. Salhab, H.M.; Ali, W.; Abboud, L. *Influence of Precipitation and Temperature on Tree-Ring Width of Brutia Pine (Pinus Brutia Ten.) in Tartous-Syria*; ACADEMIA: San Francisco, CA, USA, 2018.
29. Zhao, X.; Xia, H.; Pan, L.; Song, H.; Niu, W.; Wang, R.; Li, R.; Bian, X.; Guo, Y.; Qin, Y. Drought monitoring over Yellow River basin from 2003–2019 using reconstructed MODIS land surface temperature in Google Earth Engine. *Remote Sens.* **2021**, *13*, 3748. [CrossRef]
30. Yin, L.; Wang, L.; Keim, B.D.; Konsoer, K.; Zheng, W. Wavelet Analysis of Dam Injection and Discharge in Three Gorges Dam and Reservoir with Precipitation and River Discharge. *Water* **2022**, *14*, 567. [CrossRef]
31. Chao, L.; Zhang, K.; Wang, J.; Feng, J.; Zhang, M. A Comprehensive Evaluation of Five Evapotranspiration Datasets Based on Ground and GRACE Satellite Observations: Implications for Improvement of Evapotranspiration Retrieval Algorithm. *Remote Sens.* **2021**, *13*, 2414. [CrossRef]
32. Tiwari, A.; Shoab, M.; Dixit, A. GIS-based forest fire susceptibility modeling in Pauri Garhwal, India: A comparative assessment of frequency ratio, analytic hierarchy process and fuzzy modeling techniques. *Nat. Hazards* **2021**, *105*, 1189–1230. [CrossRef]
33. Nikhil, S.; Danumah, J.H.; Saha, S.; Prasad, M.K.; Rajaneesh, A.; Mammen, P.C.; Ajin, R.; Kuriakose, S.L. Application of GIS and AHP Method in Forest Fire Risk Zone Mapping: A Study of the Parambikulam Tiger Reserve, Kerala, India. *J. Geovis. Spat. Anal.* **2021**, *5*, 14. [CrossRef]
34. Tarboton, D.G. A new method for the determination of flow directions and upslope areas in grid digital elevation models. *Water Resour. Res.* **1997**, *33*, 309–319. [CrossRef]
35. Mafi-Gholami, D.; Zenner, E.K.; Jaafari, A. Mangrove regional feedback to sea level rise and drought intensity at the end of the 21st century. *Ecol. Indic.* **2020**, *110*, 105972. [CrossRef]
36. Mafi-Gholami, D.; Zenner, E.K.; Jaafari, A.; Bui, D.T. Spatially explicit predictions of changes in the extent of mangroves of Iran at the end of the 21st century. *Estuar. Coast. Shelf Sci.* **2020**, *237*, 106644. [CrossRef]
37. Nhu, V.-H.; Mohammadi, A.; Shahabi, H.; Ahmad, B.B.; Al-Ansari, N.; Shirzadi, A.; Clague, J.J.; Jaafari, A.; Chen, W.; Nguyen, H. Landslide susceptibility mapping using machine learning algorithms and remote sensing data in a tropical environment. *Int. J. Environ. Res. Public Health* **2020**, *17*, 4933. [CrossRef]
38. Falkowski, M.J.; Gessler, P.E.; Morgan, P.; Hudak, A.T.; Smith, A.M. Characterizing and mapping forest fire fuels using ASTER imagery and gradient modeling. *For. Ecol. Manag.* **2005**, *217*, 129–146. [CrossRef]
39. Satir, O.; Berberoglu, S.; Donmez, C. Mapping regional forest fire probability using artificial neural network model in a Mediterranean forest ecosystem. *Geomat. Nat. Hazards Risk* **2016**, *7*, 1645–1658. [CrossRef]

40. Jaafari, A. LiDAR-supported prediction of slope failures using an integrated ensemble weights-of-evidence and analytical hierarchy process. *Environ. Earth Sci.* **2018**, *77*, 42. [CrossRef]
41. Jaafari, A.; Zenner, E.K.; Pham, B.T. Wildfire spatial pattern analysis in the Zagros Mountains, Iran: A comparative study of decision tree based classifiers. *Ecol. Inform.* **2018**, *43*, 200–211. [CrossRef]
42. Xie, W.; Nie, W.; Saffari, P.; Robledo, L.F.; Descote, P.-Y.; Jian, W. Landslide hazard assessment based on Bayesian optimization–support vector machine in Nanping City, China. *Nat. Hazards* **2021**, *109*, 931–948. [CrossRef]
43. Jaafari, A.; Pourghasemi, H.R. Factors Influencing Regional-Scale Wildfire Probability in Iran: An Application of Random Forest and Support Vector Machine. In *Spatial Modeling in GIS and R for Earth and Environmental Sciences*; Elsevier: Amsterdam, The Netherlands, 2019; pp. 607–619.
44. Zhang, K.; Shalehy, M.H.; Ezaz, G.T.; Chakraborty, A.; Mohib, K.M.; Liu, L. An integrated flood risk assessment approach based on coupled hydrological-hydraulic modeling and bottom-up hazard vulnerability analysis. *Environ. Model. Softw.* **2022**, *148*, 105279. [CrossRef]
45. Wang, S.; Zhang, K.; Chao, L.; Li, D.; Tian, X.; Bao, H.; Chen, G.; Xia, Y. Exploring the utility of radar and satellite-sensed precipitation and their dynamic bias correction for integrated prediction of flood and landslide hazards. *J. Hydrol.* **2021**, *603*, 126964. [CrossRef]
46. Geng, M.; Ma, K.; Sun, Y.; Wo, X.; Wang, K. Changes of land use/cover and landscape in Zhalong wetland as "red-crowned cranes country", Heilongjiang province, China. *Glob. NEST J.* **2020**, *22*, 477–483.
47. Jaafari, A.; Zenner, E.K.; Panahi, M.; Shahabi, H. Hybrid artificial intelligence models based on a neuro-fuzzy system and metaheuristic optimization algorithms for spatial prediction of wildfire probability. *Agric. For. Meteorol.* **2019**, *266–267*, 198–207. [CrossRef]
48. Zhang, K.; Ali, A.; Antonarakis, A.; Moghaddam, M.; Saatchi, S.; Tabatabaeenejad, A.; Chen, R.; Jaruwatanadilok, S.; Cuenca, R.; Crow, W.T. The sensitivity of North American terrestrial carbon fluxes to spatial and temporal variation in soil moisture: An analysis using radar-derived estimates of root-zone soil moisture. *J. Geophys. Res. Biogeosci.* **2019**, *124*, 3208–3231. [CrossRef]
49. Veena, H.S.; Ajin, R.S.; Loghin, A.-M.; Sipai, R.; Adarsh, P.; Viswam, A.; Vinod, P.G.; Jacob, M.K.; Jayaprakash, M. Wildfire risk zonation in a tropical forest division in Kerala, India: A study using geospatial techniques. *Int. J. Conserv. Sci.* **2017**, *8*, 475–484.
50. Jaafari, A.; Pazhouhan, I.; Bettinger, P. Machine Learning Modeling of Forest Road Construction Costs. *Forests* **2021**, *12*, 1169. [CrossRef]
51. Salloum, J.; Abdo, H. Statistical modeling of conservation the vegetation of the land in Alqadmous area from rainfall erosion. *Tishreen Univ. J. Res. Sci. Stud.-Arts Hum. Ser.* **2016**, *38*, 667–683.
52. Li, J.; Zhao, Y.; Zhang, A.; Song, B.; Hill, R.L. Effect of grazing exclusion on nitrous oxide emissions during freeze-thaw cycles in a typical steppe of Inner Mongolia. *Agric. Ecosyst. Environ.* **2021**, *307*, 107217. [CrossRef]
53. Jaafari, A.; Gholami, D.M.; Zenner, E.K. A Bayesian modeling of wildfire probability in the Zagros Mountains, Iran. *Ecol. Inform.* **2017**, *39*, 32–44. [CrossRef]
54. Fornacca, D.; Ren, G.; Xiao, W. Evaluating the best spectral indices for the detection of burn scars at several post-fire dates in a mountainous region of Northwest Yunnan, China. *Remote Sens.* **2018**, *10*, 1196. [CrossRef]
55. Shabani, S.; Najafi, A.; Majnonian, B.; Alavi, J.; Sattarian, A. Spatial prediction of soil disturbance caused by forest logging using generalized additive models and GIS. *Eur. J. For. Res.* **2019**, *138*, 595–606. [CrossRef]
56. Masinda, M.M.; Sun, L.; Wang, G.; Hu, T. Moisture content thresholds for ignition and rate of fire spread for various dead fuels in northeast forest ecosystems of China. *J. For. Res.* **2021**, *32*, 1147–1155. [CrossRef]
57. Zhang, K.; Wang, S.; Bao, H.; Zhao, X. Characteristics and influencing factors of rainfall-induced landslide and debris flow hazards in Shaanxi Province, China. *Nat. Hazards Earth Syst. Sci.* **2019**, *19*, 93–105. [CrossRef]
58. Kayet, N.; Chakrabarty, A.; Pathak, K.; Sahoo, S.; Dutta, T.; Hatai, B.K. Comparative analysis of multi-criteria probabilistic FR and AHP models for forest fire risk (FFR) mapping in Melghat Tiger Reserve (MTR) forest. *J. For. Res.* **2020**, *31*, 565–579. [CrossRef]
59. Abedi Gheshlaghi, H. Using GIS to develop a model for forest fire risk mapping. *J. Indian Soc. Remote Sens.* **2019**, *47*, 1173–1185. [CrossRef]
60. Sahana, M.; Ganaie, T.A. GIS-based landscape vulnerability assessment to forest fire susceptibility of Rudraprayag district, Uttarakhand, India. *Environ. Earth Sci.* **2017**, *76*, 676. [CrossRef]
61. Mohammed, S.; Hassan, E.; Abdo, H.G.; Szabo, S.; Mokhtar, A.; Alsafadi, K.; Al-Khouri, I.; Rodrigo-Comino, J. Impacts of rainstorms on soil erosion and organic matter for different cover crop systems in the western coast agricultural region of Syria. *Soil Use Manag.* **2021**, *37*, 196–213. [CrossRef]
62. Wang, X.; Zhang, Y.; Luo, M.; Xiao, K.; Wang, Q.; Tian, Y.; Qiu, W.; Xiong, Y.; Zheng, C.; Li, H. Radium and nitrogen isotopes tracing fluxes and sources of submarine groundwater discharge driven nitrate in an urbanized coastal area. *Sci. Total Environ.* **2021**, *763*, 144616. [CrossRef]
63. Kanga, S.; Tripathi, G.; Singh, S.K. Forest fire hazards vulnerability and risk assessment in Bhajji forest range of Himachal Pradesh (India): A geospatial approach. *J. Remote Sens. GIS* **2017**, *8*, 1–16.
64. Abdo, H. Assessment of landslide susceptibility zonation using frequency ratio and statistical index: A case study of Al-Fawar basin, Tartous, Syria. *Int. J. Environ. Sci. Technol.* **2022**, *19*, 2599–2618. [CrossRef]
65. Jaafari, A.; Najafi, A.; Pourghasemi, H.R.; Rezaeian, J.; Sattarian, A. GIS-based frequency ratio and index of entropy models for landslide susceptibility assessment in the Caspian forest, northern Iran. *Int. J. Environ. Sci. Technol.* **2014**, *11*, 909–926. [CrossRef]

66. Jaafari, A.; MafiGholami, D. Wildfire hazard mapping using an ensemble method of frequency ratio with Shannon's entropy. *Iran. J. For. Poplar Res.* **2017**, *25*, 232–243.
67. Setiawan, I.; Mahmud, A.R.; Mansor, S.; Shariff, A.R.M.; Nuruddin, A.A. GIS-grid-based and multi-criteria analysis for I dentifying and mapping peat swamp forest fire hazard in Pahang, Malaysia. *Disaster Prev. Manag. Int. J.* **2004**, *13*, 379–386. [CrossRef]
68. Hossain, M.K.; Meng, Q. A fine-scale spatial analytics of the assessment and mapping of buildings and population at different risk levels of urban flood. *Land Use Policy* **2020**, *99*, 104829. [CrossRef]
69. Jaafari, A.; Najafi, A.; Melón, M.G. Decision-making for the selection of a best wood extraction method: An analytic network process approach. *For. Policy Econ.* **2015**, *50*, 200–209. [CrossRef]
70. TL, S. The Analytic Hierarchy Process, Planning, Priority Setting. In *Resource Allocation*; McGraw-Hill International Book Company: New York, NY, USA, 1980.
71. Pham, B.T.; Jaafari, A.; Phong, T.V.; Yen, H.P.H.; Tuyen, T.T.; Luong, V.V.; Nguyen, H.D.; Le, H.V.; Foong, L.K. Improved flood susceptibility mapping using a best first decision tree integrated with ensemble learning techniques. *Geosci. Front.* **2021**, *12*, 101105. [CrossRef]
72. Pham, B.T.; Jaafari, A.; Van Phong, T.; Mafi-Gholami, D.; Amiri, M.; Van Tao, N.; Duong, V.-H.; Prakash, I. Naïve Bayes ensemble models for groundwater potential mapping. *Ecol. Inform.* **2021**, *64*, 101389. [CrossRef]
73. Tran, Q.C.; Minh, D.D.; Jaafari, A.; Al-Ansari, N.; Minh, D.D.; Van, D.T.; Nguyen, D.A.; Tran, T.H.; Ho, L.S.; Nguyen, D.H. Novel Ensemble Landslide Predictive Models Based on the Hyperpipes Algorithm: A Case Study in the Nam Dam Commune, Vietnam. *Appl. Sci.* **2020**, *10*, 3710. [CrossRef]
74. Jaafari, A.; Panahi, M.; Mafi-Gholami, D.; Rahmati, O.; Shahabi, H.; Shirzadi, A.; Lee, S.; Bui, D.T.; Pradhan, B. Swarm intelligence optimization of the group method of data handling using the cuckoo search and whale optimization algorithms to model and predict landslides. *Appl. Soft Comput.* **2022**, *116*, 108254. [CrossRef]
75. Shang, K.; Chen, Z.; Liu, Z.; Song, L.; Zheng, W.; Yang, B.; Liu, S.; Yin, L. Haze Prediction Model Using Deep Recurrent Neural Network. *Atmosphere* **2021**, *12*, 1625. [CrossRef]
76. Yin, L.; Wang, L.; Huang, W.; Tian, J.; Liu, S.; Yang, B.; Zheng, W. Haze Grading Using the Convolutional Neural Networks. *Atmosphere* **2022**, *13*, 522. [CrossRef]
77. Gholamnia, K.; Gudiyangada Nachappa, T.; Ghorbanzadeh, O.; Blaschke, T. Comparisons of Diverse Machine Learning Approaches for Wildfire Susceptibility Mapping. *Symmetry* **2020**, *12*, 604. [CrossRef]
78. Tshering, K.; Thinley, P.; Shafapour Tehrany, M.; Thinley, U.; Shabani, F. A comparison of the qualitative analytic hierarchy process and the quantitative frequency ratio techniques in predicting forest fire-prone areas in Bhutan using GIS. *Forecasting* **2020**, *2*, 36–58. [CrossRef]
79. Gülçin, D.; Deniz, B. Remote sensing and GIS-based forest fire risk zone mapping: The case of Manisa, Turkey. *Turk. J. For.* **2020**, *21*, 15–24. [CrossRef]
80. Suryabhagavan, K.; Alemu, M.; Balakrishnan, M. GIS-based multi-criteria decision analysis for forest fire susceptibility mapping: A case study in Harenna forest, southwestern Ethiopia. *Trop. Ecol.* **2016**, *57*, 33–43.
81. Eugenio, F.C.; dos Santos, A.R.; Fiedler, N.C.; Ribeiro, G.A.; da Silva, A.G.; dos Santos, Á.B.; Paneto, G.G.; Schettino, V.R. Applying GIS to develop a model for forest fire risk: A case study in Espírito Santo, Brazil. *J. Environ. Manag.* **2016**, *173*, 65–71. [CrossRef]
82. Abdo, H.G. Estimating water erosion using RUSLE, GIS and remote sensing in Wadi-Qandeel river basin, Lattakia, Syria. *Proc. Indian Natl. Sci. Acad.* **2021**, *87*, 514–523. [CrossRef]
83. Abdo, H.G. Evaluating the potential soil erosion rate based on RUSLE model, GIS, and RS in Khawabi river basin, Tartous, Syria. *DYSONA-Appl. Sci.* **2022**, *3*, 24–32.